ICAS 2020 SHANGHAI
International Council of the Aeronautical Sciences
32nd Congress of the International Council of the Aeronautical Sciences
September 6-10, 2021
Pudong Shangri-La, Shanghai, China

TRANSITION PREDICTION FOR TRANSPORT AIRCRAFT CONFIGURATIONS BASED ON OVERSET GRID

Du Yiming[1], Gao Zhenghong[2], Pang Chao[2]

[1] College of Aerospace Engineering, Shenyang Aerospace University, Shenyang China, 110137
[2]School of Aeronautics, Northwestern Polytechnical University, Xi'an China, 710072

Abstract

Laminar-flow aerodynamic design receives great importance by the civil aviation field in recent years. Complex flight conditions and complex configurations give challenges to present CFD techniques especially the transition prediction method and grid generation. This work adopted $\gamma - \tilde{R}e_{\theta t}$ local correlation-based transition model and overset meshing strategy to conduct flow simulations of typical civil transport aircraft configurations. A locally helicity-based modeling method for crossflow instability was introduced to extend the three-dimensional transition prediction ability. Results have shown well behavior of the crossflow-extended transition model on surface pressure and force prediction at transonic cruise Mach number. Combining structured overset grid, crossflow-extended transition model can also give better prediction on transition characteristics of the high-lift configuration compared to the baseline transition model. However, high Reynolds number of actual flight condition seemed to exceed the application boundary of present local transition model. Although the predicted pressure coefficient distributions were in good agreement with the experiment results, the predicted transition line was far forward to the leading edge.

Keywords: boundary-layer transition prediction; crossflow instability; overset grid; transport aircraft; high Reynolds number

1. Introduction

The development of high-efficiency aircraft puts forward higher requirements for aerodynamic design engineering [1]. Among all related fields, laminar conceptual/shape design and control offers the potential for improvements in aircraft fuel usage, range or endurance that far exceed any known single aeronautical technology [2]. Therefore, how to more accurately simulate the boundary-layer transition as well as its influence on aerodynamic characteristics is the main challenge for computational fluid dynamics (CFD) application. In recent years, CFD technology based on Reynolds-Averaged Navier-Stokes (RANS) method with local correlation-based transition model [3] such as $\gamma - \tilde{R}e_{\theta t}$ model [4] is more and more used in practice. However, the influence from complex application conditions and complex configuration in the field of civil transport aircraft design are still the key problems affecting the application of transition models. In addition, it is still necessary to improve the three-dimensional transition prediction ability of the model to meet the requirements of actual aircraft laminar flow design.

Actual laminar flow design of aircraft engineering generally needs to consider the laminar flow characteristics of multiple flight conditions (such as high-speed cruise and low-speed climb conditions) at the same time [5], which makes the CFD transition prediction must have the ability to deal with complex mechanisms. Although $\gamma - \tilde{R}e_{\theta t}$ transition model can accurately predict natural transition, bypass transition and separation-induced transition, its transition criterion and empirical correlations are established by theory, experiment and experience of low-speed (incompressible) and low-Reynolds-number (order of millions) flow. Therefore, it naturally has a certain application boundary.

Whether it can be applied at high Mach number (transonic) and high Reynolds number (order of ten millions) conditions of high-speed civil aircraft still needs to be verified. This work is inadequate at present.

In addition, complex flow phenomena in actual flight also put forward higher requirements for the comprehensive application ability of transition model. Taking the high-lift flow as an example. Except for boundary-layer transition, there are many other phenomena such as, wake/boundary layer blending, recirculation, tip vortex and possible separation at high angles of attack. These flow phenomena may affect the prediction ability of the transition model. In addition, complex configurations also bring difficulties to mesh generation. Grid overlapping, also known as the overset-grid method or chimera technique, requires neither one-to-one connectivity nor a shared interface to transfer information from one zone to another [6]. Single grid zone can be generated independently for an individual part according to the particular geometry and then assembled together, which integrates the advantages of different type of grid topologies, e.g. body-fitted grid for surface and Cartesian grid for farfield. Furthermore, for aerodynamic optimization, this simple topology is friendly to the frequent operation of mesh deforming with little damage to grid orthogonality. Therefore, overset technique has been implemented by more and more commercial or in-house solvers as a selectable meshing capability [7].

Finally, in actual flight, the three-dimensional flow characteristics will introduce more transition mechanisms, involving inviscid instability, roughness effect and turbulent boundary layer pollution from the leading edge. At the same time, the interaction of two-dimensional transition mechanisms, e.g. Tollmien-Schlichting (T-S) [8] instabilities, also makes it difficult to carry out three-dimensional transition modeling and prediction. Original $\gamma - \tilde{R}e_{\theta t}$ transition model is proposed for two-dimensional transition mechanism, so it is not suitable for three-dimensional boundary-layer transition prediction, especially for configurations with large sweep angle. Taking crossflow (CF) transition [9] as an example. The occurrence of third dimension leads to the existence of pressure gradient in spanwise direction, and induces crossflow instability, which is likely to trigger transition prior to two-dimensional instabilities. However, the modeling and application of three-dimensional crossflow transition are not sufficient at present. Most of the existing crossflow transition models adopt the empirical C1 criteria or the more physical C2 criteria proposed by Arnal et al. [9], and use the approximate integral thickness and velocity profile obtained by three-dimensional boundary layer Falkner-Scan-Cook (FSC) equation [10]. However, this method can only be applied to favorable pressure gradient and swept wing configurations with infinite span or high aspect ratio. Methods or criterion that suitable for crossflow transition prediction on arbitrary shape are in great urgent.

This paper makes effort to deal with the above-mentioned challenges in the field of CFD application on civil transport aircraft laminar flow design. Section 2 introduces the overset meshing strategy that suitable for grid generation of complex configurations and local transition modeling method on stationary crossflow instabilities for arbitrary shapes. Validation cases are also present. Section 3 gives applications and discussions of these methods on three typical transport aircraft configurations that proposed in recent years. Main conclusions and prospects are finally made in Section 4.

2. Prediction Methods and Validations

2.1 Solver

The solver adopted in this paper is the NASA CFL3D [11] code, which has been released on GitHub by NASA in 2017. CFL3D was developed as a cell-based RANS code for structured grid based on finite volume formulation, supporting both 1-1 blocking and overset topologies, with several turbulence model can be selected. The overset capability was included from the initial development stage, while the transition prediction module was integrated in recent versions. In this paper, the convective and pressure terms of RANS equations are solved by Roe's flux difference splitting (FDS) scheme, while the viscous terms by central difference scheme. To promote the computation efficiency,

mesh sequence and multigrid acceleration techniques are also used. The following 2003 version of *k-ω* SST model [12] is adopted for fully-turbulent computation and coupling with transition model. More details of this model can be referred to in Ref. [12].

$$\frac{\partial k}{\partial t}+U_j\frac{\partial k}{\partial x_j}=\dot{P}_k-D_k+\frac{\partial}{\partial x_j}\left[\left(\nu+\frac{\nu_T}{\sigma_k}\right)\frac{\partial k}{\partial x_j}\right] \tag{1}$$

$$\frac{\partial \omega}{\partial t}+U_j\frac{\partial \omega}{\partial x_j}=\alpha\frac{\omega}{k}R_{ij}\frac{\partial U_i}{\partial x_j}-\beta\omega^2+\frac{\partial}{\partial x_j}\left[(\nu+\sigma_\omega\nu_T)\frac{\partial \omega}{\partial x_j}\right]+(1-F_1)\frac{2\sigma_{\omega 2}}{\omega}\frac{\partial k}{\partial x_j}\frac{\partial \omega}{\partial x_j} \tag{2}$$

$$R_{ij}=2\nu_T\left(S_{ij}-\frac{1}{3}\frac{\partial U_k}{\partial x_k}\delta_{ij}\right)-\frac{2}{3}k\delta_{ij} \tag{3}$$

$$P_k=R_{ij}S_{ij}\approx 2\nu_T S_{ij}S_{ij}=\nu_T S^2,\qquad D_k=\beta^* k\omega \tag{4}$$

$$\dot{P}_k=min(P_k,\ 10\cdot D_k) \tag{5}$$

2.2 Overset Grid Technique

The overset implementation used in CFL3D solver is based on the method proposed by Benek et al [13]. The key step for overset grid is grid assembly, which contains hole cutting and interpolation. Hole cutting is to “remove” certain points on specific grid from computation at which it immerses into solid walls. Any point that located within the hole area is termed “hole point”. Interpolation is to determine the boundaries with no specific boundary conditions that need data transfer from “target cells” in overlapping grid. This type of boundary includes “fringe points” that border hole points, and “outer boundary points” of an internal overlapping grid. All the hole, fringe and outer boundary points are set *iblank* 0 in PLOT3D format for computation exemption. Other points for normal computation are designated “field points” with *iblank* marked 1. Since CFL3D is a cell-centered solver with maximum third-order spatial differencing at cell interfaces (i.e., grid lines), the fringe points refer to every first two cells around the hole border points both vertically and horizontally. Similarly, the outer boundary points for body-fitted grid and inner box should also occupy at least 2 cell layers. These points obtain data from specific target cells in field points of overlapping grid with trilinear interpolation. It’s worth noting that two grids that need information transfer should possess similar grid size and enough overlapping area at interpolation regions, otherwise the target cell searching would result in some orphan/illegal points or even fail. CFL3D provides an individual code called MultiGeometry Grid Embedder (MaGGiE) [14] to make grid assembly. MaGGiE needs user-specified index information to get preliminary definition of holes and outer boundaries, so it is not very convenience for three-dimensional grids.

To validate the overset grid ability as well as the basic turbulence model in CFL3D, China Transport 1 (CHN-T1) [15] configuration at fixed transition (fully-turbulent) condition is selected as a test case. CHN-T1 is a single-channel civil passenger aircraft, which is developed by China Aerodynamic Research and Development Center (CARDC). It is also the research model of the 1st Aeronautical CFD Credibility Workshop (AeCW-1) in China. This configuration has been tested in wind tunnel since 2013 [16]. The medium-sized overset grid generated by this paper [17] is shown in Fig. 1. The whole computational domain consists of 20 grid blocks (18 body-fitted blocks and 2 farfield blocks) with a total cell amount of 1.45 million, which is close to that of the medium-size 1-1-blocking grid provided by the AeCW-1 committee. To generate the surface mesh of fuselage and wings, the transfinite interpolation (TFI) method is used, and then the Thomas-Middlecoff method is used to iterate the elliptic equation until the maximum residual value is reduced to 5×10^{-6}; The surface mesh of nose, tail, tip and wing-body junction is obtained by solving hyperbolic equations; All the body-fitted grids are obtained by solving hyperbolic equations along the normal direction of the surface. These methods can ensure mesh orthogonality near the surface and the whole quality of the grid. The farfield Cartesian grids include an inner and an outer block. In order to better assemble the grid, the inner block is properly refined near the body so that the grid spacing is slightly less than that of the outer layer of body-fitted grids at the overlapping zones.

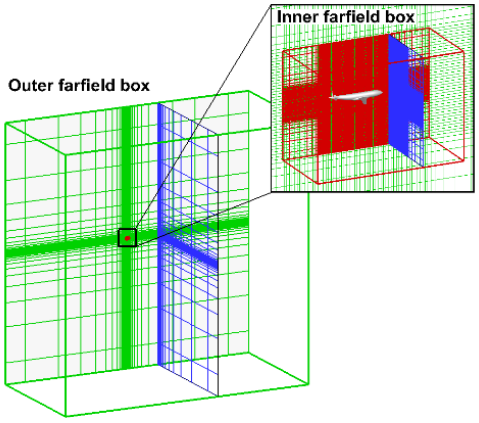

(a) Farfield Cartesian blocks

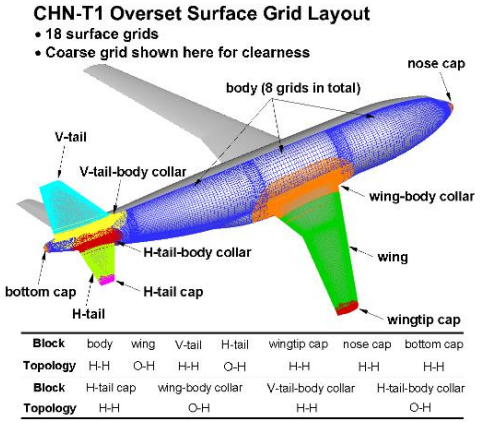

(b) Surface grid overlapping

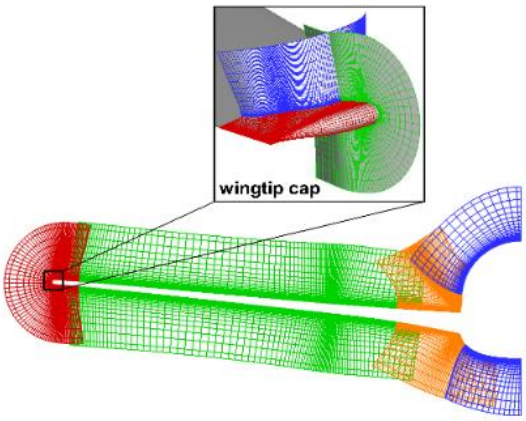

(c) Grid distribution at streamwise section and wingtip

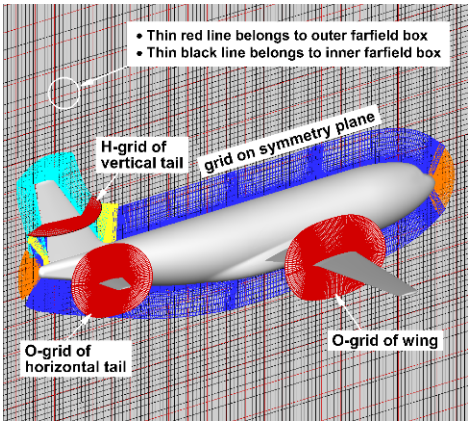

(d) Grid overlapping distribution at symmetry plane

Figure 1 – Overset grid of CHN-T1 configuration.

The computation conditions are Ma=0.78, Re=3.3×10^6 and $C_{L,target}$=0.5. Fig. 2 shows the comparison of computational force and pressure coefficients with experiment or reference data. Since the wind-tunnel test [16] did not obtain surface characteristic, the pressure coefficient result by CARDC TRIP 3.0 solver on 10.4 billion grid [18] is taken as reference. It can be found that the lift and lift-drag polar curves obtained by both committee 1-1-blocking and overset grids are in good agreement with the experimental value. However, for pressure distribution at η=85% spanwise section, the overset grid obviously can obtain more accurate shock wave compared to that of committee 1-1-blocking grid due to the denser grid distribution on and near the surfaces. This is exactly the advantage of overset meshing strategy.

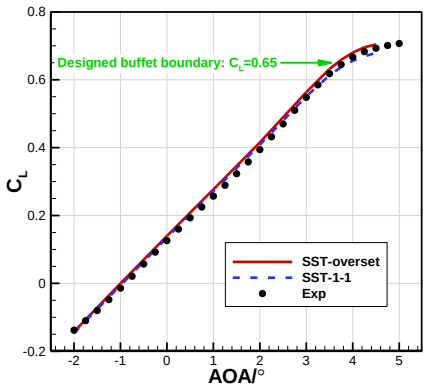

(a) Lift curve

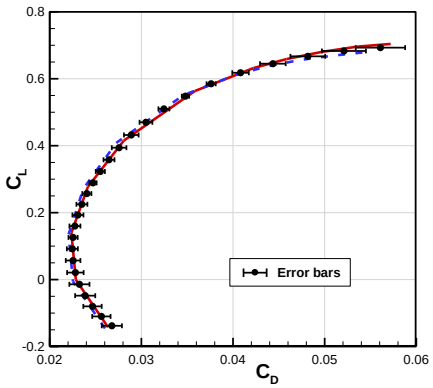

(b) Lift-drag polar curve

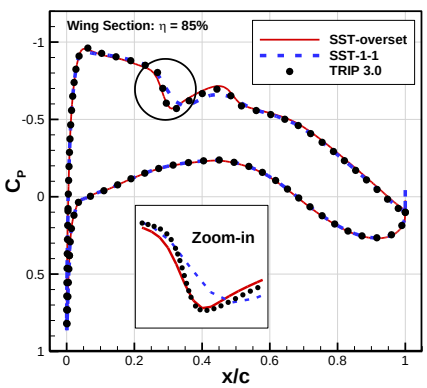

(c) Pressure coefficient distribution

Figure 2 – Computational force and pressure coefficients of overset and 1-1-blocking grids comparing with experiment or reference CFD data.

2.3 Transition Model with Crossflow Instability Effect

As shown in Fig. 3, for three-dimensional transonic and low Mach number flows, the boundary-layer instability mechanisms in actual flight basically results from four basic modes [19]-[21], namely, basic two-dimensional T-S instability, CF instability due to three-dimensional effect, attachment-line instability or leading-edge contamination caused by fuselage turbulent boundary layer, and centrifugal instability caused by curvature (also known as Görtler instability). Generally speaking, the leading-edge contamination and Görtler instability can be eliminated by proper shape design. Therefore, the crossflow instability is the main transition mechanisms in three-dimensional. For low-turbulence-intensity flow at high altitude or wind tunnel, stationary crossflow instabilities/vortices are the dominant mechanism [22].

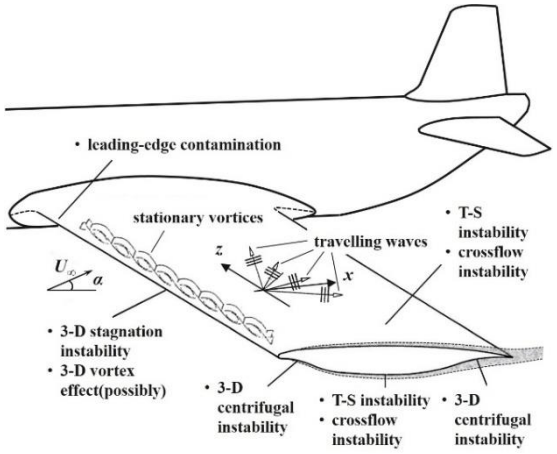

Figure 3 – Possible instability mechanisms in actual flight.

A well-arranged explanation of stationary crossflow instability mechanism can be found in Ref. [23] by the author. In recent years, a crossflow transition modeling method based on local correlation transition model framework has been deeply discussed and developed [24]-[26]. In this method, helicity *He*, a locally defined variable also known as streamwise vorticity, is used to measure the strength of the stationary crossflow vortices in boundary layer. The formulations of helicity and the crossflow transition criteria using related Reynolds number are as follows

$$He = \Omega_{streamwise} = \frac{\boldsymbol{u}}{|\boldsymbol{u}|} \cdot \boldsymbol{\omega} \tag{6}$$

$$\frac{Re_{He,max}}{Re_{He,t}} = 1 \tag{7}$$

where

$$\frac{\boldsymbol{u}}{|\boldsymbol{u}|} = \left(\frac{u}{\sqrt{u^2+v^2+w^2}}, \frac{v}{\sqrt{u^2+v^2+w^2}}, \frac{w}{\sqrt{u^2+v^2+w^2}}\right) \tag{8}$$

$$\boldsymbol{\omega} = \nabla \times \boldsymbol{u} = \left(\frac{\partial w}{\partial y} - \frac{\partial v}{\partial z}, \frac{\partial u}{\partial z} - \frac{\partial w}{\partial x}, \frac{\partial v}{\partial x} - \frac{\partial u}{\partial y}\right) \tag{9}$$

A detailed physical rationality analysis and the derivation of the above equations are introduced in Ref. [27] by the author. Since the assumption of infinite swept wing is not introduced into the modeling process, it is suitable for crossflow transition prediction with arbitrary shape as well as adverse pressure gradient. The baseline $\gamma - \tilde{R}e_{\theta t}$ transition model,

$$\frac{\partial(\rho \tilde{R}e_{\theta t})}{\partial t} + \frac{\partial(\rho U_j \tilde{R}e_{\theta t})}{\partial x_j} = P_{\theta t} + \frac{\partial}{\partial x_j}\left[\sigma_{\theta t}(\mu + \mu_T)\frac{\partial \tilde{R}e_{\theta t}}{\partial x_j}\right] \tag{10}$$

$$\frac{\partial(\rho\gamma)}{\partial t} + \frac{\partial(\rho U_j \gamma)}{\partial x_j} = P_\gamma + P_{\gamma,CF} - E_\gamma + \frac{\partial}{\partial x_j}\left[\left(\mu + \frac{\mu_T}{\sigma_\gamma}\right)\frac{\partial \gamma}{\partial x_j}\right] \tag{11}$$

$$P_{\theta t} = c_{\theta t}\frac{\rho}{t}\left(Re_{\theta t} - \tilde{R}e_{\theta t}\right)(1 - F_{\theta t}) \tag{12}$$

$$P_{\gamma} = F_{length}c_{a1}\rho S(\gamma \cdot F_{onset})^{0.5}(1 - c_{e1}\gamma) \tag{13}$$

$$E_{\gamma} = F_{turb}c_{a2}\rho\Omega\gamma(c_{e2}\gamma - 1) \tag{14}$$

couples with *k*-*ω* SST model Eqn. (1)-(5) as

$$\gamma_{eff} = max\left(\gamma, \gamma_{sep}\right) \tag{15}$$

$$\tilde{P}_k = \gamma_{eff}\dot{P}_k \tag{16}$$

$$\tilde{D}_k = min\left(max\left(\gamma_{eff}, 0.1\right), 1.0\right)D_k \tag{17}$$

The crossflow transition extension is

$$P_{\gamma,CF} = F_{length,CF}c_{a1}\rho S\left(\gamma \cdot F_{onset,CF}\right)^{0.5}(1 - c_{e1}\gamma) \tag{18}$$

$$F_{onset,CF} = \max\left(F_{onset2,CF} - F_{onset3,CF}, 0.0\right) \tag{19}$$

$$F_{onset3,CF} = \max\left[1 - \left(\frac{R_T}{2}\right)^3, 0.0\right] \tag{20}$$

$$F_{onset2,CF} = \min\left[\max\left(F_{onset1,CF}, F_{onset1,CF}^4\right), 2.0\right] \tag{21}$$

$$F_{onset1,CF} = \frac{Re_{He,max}}{C \cdot Re_{He,t}}, C = 0.7 \tag{22}$$

$$F_{length,CF} = 5.0 \tag{23}$$

Detail definitions and origin of the above variables and constants can be found in Ref. [4] and [24].

The validity of crossflow-extended transition model is verified on the NLF(2)-0415 infinite wing, which is designed for low speed and low drag (laminar flow) general aircraft without swept back. The experiment of 45° swept-back configuration [21] was carried out in the unsteady wind tunnel of Arizona State University. Because the left and right walls of the wind tunnel (opposite to the upper and lower surfaces of the wing) are close to the model, the wind tunnel is included in the grid to accurately reflect the influence on pressure gradient in this problem. The computational grid is shown in Fig. 4. The wing deflects 4° anticlockwise as the angle of attack to make the incoming flow keep parallel to the tunnel walls. The sweep angle is considered by setting 45° sideslip angle of the wing, and periodic boundary conditions are set at both ends of the wing span to realize the assumption of infinite span. For *α*=-4° which we choose, the lowest pressure occurs at about 71% chord length, and the long favorable pressure gradient enhances the stationary crossflow vortices, while other instabilities are in subcritical state. The computational conditions are listed in Table 1. Six different Reynolds number conditions are computed, and the Mach number is always incompressible.

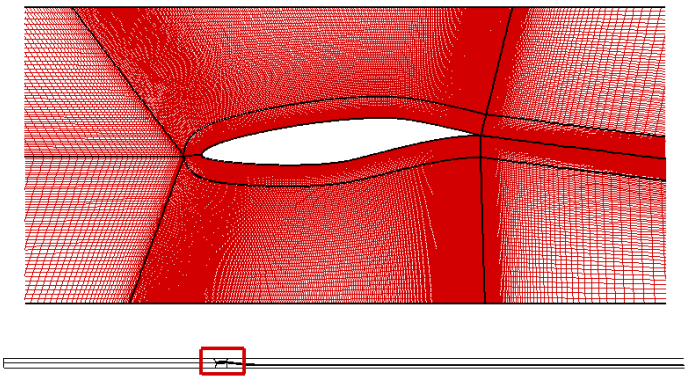

Figure 4 – Computational grid of NLF(2)-0415 infinite-span swept wing.

Table 1 – Test cases of NLF(2)-0415 infinite-span swept wing.

	α/°	β/°	Wind tunnel wall		Tu_{inf}	μ_{Tinf}/μ
	-4	45	Included		0.09%	1.0
Ma	0.123	0.14	0.151	0.174	0.209	0.239
***Re*/10^6**	1.921	2.191	2.37	2.73	3.27	3.73

Fig. 5 shows the comparison of the pressure gradient obtained by using the wind-tunnel grid (Fig. 4) and the freestream grid with the experiment data. It can be found that there exist obvious differences in the pressure distribution between the two different conditions. The wind-tunnel grid used in this paper can correctly reflect the pressure gradient in the transition experiment. Fig. 6 shows the predicted transition onset locations (TOL) by different models comparing with the experiment results from naphthalene sublimation, hot film and hot wire. It can be found that the TOLs by different experiment methods move forward (to the leading edge) with the increase of Reynolds number. The baseline $\gamma - \tilde{R}e_{\theta t}$ model predicts almost constant TOLs with increasing Reynolds number since there is no mechanism to trigger T-S wave transition under continuous favorable pressure gradient. On the contrary, the crossflow-extended transition model can get the same trend as the experiment, which demonstrates the effectiveness of the crossflow transition criteria introduced in this section.

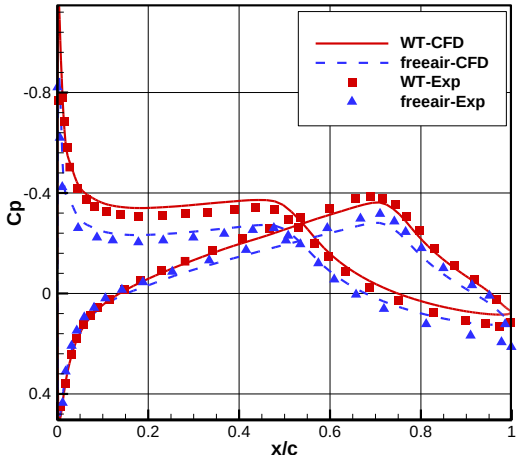

Figure 5 – C_p comparison of wind-tunnel and freestream cases with experiment results.

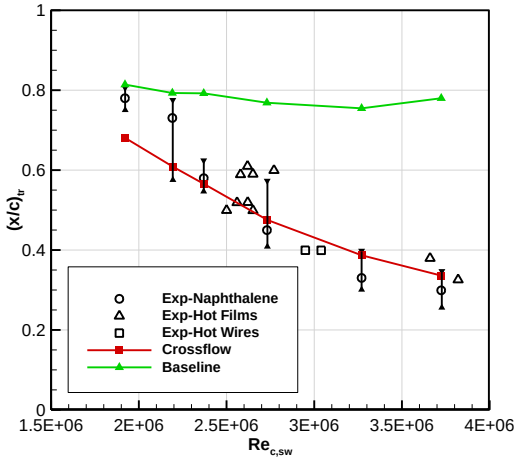

Figure 6 – Comparison of predicted transition onset location from different models.

3. Results and Discussions

In this section, transition characteristics of three typical civil transport aircraft configurations are studied. For the convenience of forthcoming discussion, the computational conditions of all the configurations are summarized in Table 2.

Table 2 – Computational conditions of different configurations.

Configuration	***Ma***	***Re*/10^6**	α/°	Tu_{inf}	μ_{Tinf}/μ
CHN-T1	0.7	3.3	0.1	0.8%	5.0
Trap Wing	0.2	4.3	13.0	0.075%	0.1
CRM-NLF	0.8565	14.946	1.98031	0.24%	12.0

3.1 CARDC CHN-T1 Configuration

The experiment result of the condition listed in Table 2 was obtained by CARDC FL-26 wind tunnel [16]. The experiment did not carry out flow visualization, so only force coefficients of free and fixed transition are available. The skin friction coefficient prediction results of the baseline and crossflow-extended transition model are shown in Fig. 7. It can be seen that the stronger crossflow effect of the

inner wing [28][29] has been basically predicted by the crossflow-extended model, and the transition behavior of the fuselage head is similar to the experiment results in DLR 6:1 prolate inclined spheroid [30], especially the forward transition near the leeward attachment line. In terms of force coefficient (Table 3), the drag prediction of the crossflow-extended transition model are closer to those of free transition experiment, but the lift coefficients of both models are closer to that of fixed transition experiment, which has no clear reason yet.

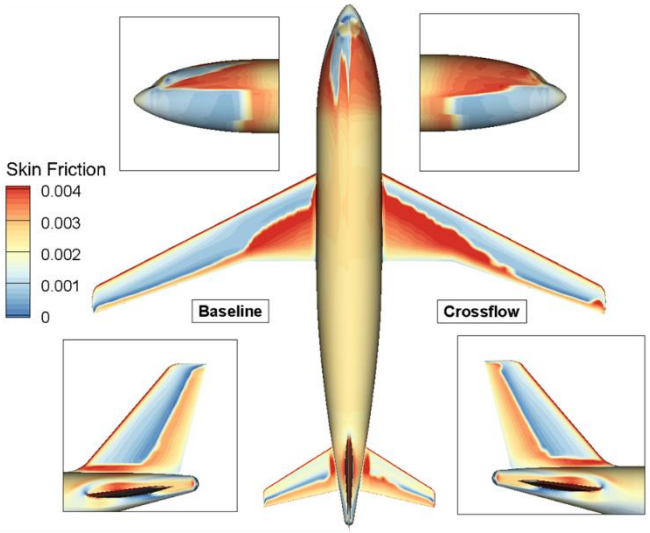

Figure 7 – Comparison of skin friction coefficient distribution from different models.

Table 3 – Comparison of computational forces from different models with experiment.

	C_L	C_D
CARDC FL-26 2.4m×2.4m Wind Tunnel (*Tu*=0.8%)		
Exp.(Fixed transition)	**0.1522**	0.02135
Exp.(Free transition)	0.1827	**0.01874**
Fully-turbulent	0.1463	0.02143
Baseline model	0.1633	0.01790
Crossflow-extended model	**0.1580**	**0.01850**

3.2 NASA Trap Wing High-Lift Configuration

NASA trapezoidal (Trap) wing is a three-stage swept wing configuration discussed in the first AIAA High Lift Prediction Workshop (HiLiftPW-1) [31][32]. In this case, 25° landing flap deflection state, i.e. HiLiftPW-1 Configuration 1 with no brackets is selected. Therefore, it is impossible to obtain the "wavy" prediction results similar to those in experiments. Eliasson et al. [33] used the e^N method to study the transition characteristic of the model, and the critical *N* value was in the range of 5~10. The results showed that a higher *N* value can get better TOL prediction that consistent with the experiment. Due to the problem of hot film arrangement in NASA Trap Wing transition experiment, it is difficult to judge the TOL in some regions [32]. Therefore, the organizing committee of HiLiftPW-1 suggested that the numerical results from Eliasson et al. [33] be used as a reference for CFD calculation.

Crippa and krimmelbein [34] used DLR TAU solver to analyze the stability of this configuration. They distinguished the transition mechanism by means of double *N* strategy, where N_{TS}=N_{CF}=8.5. At α=13°, the general transition pattern (Fig. 8) is similar to that of Eliasson et al. (*N*=10) [33]. Based on Crippa and krimmelbein [34], the transition is dominated by crossflow instabilities on the lower surface of main wing. In Fig. 9, shin friction coefficient distributions of two reference results are introduced (small pictures with black border). Rumsey and Lee Rausch [35] used the committee 1-1-blocking grid and $\gamma - \tilde{R}e_{\theta t}$ transition model to simulate the transition by CFL3D, but the predicted result of the main wing lower surface was significantly different from that of Eliasson et al. (*N*=10) or Crippa and

krimmelbein. While Sclafani et al. [36] used overset grid and $\gamma - \tilde{R}e_{\theta t}$ transition model in NASA OVERFLOW solver, but no transition (fully turbulence) was predicted on the lower surface of main wing. It is worth noting that the selection of critical *N* factor by Ref. [33] and [34] were empirical, so the real transition mechanism is questionable. However, it at least shows the transition prediction challenge in this region.

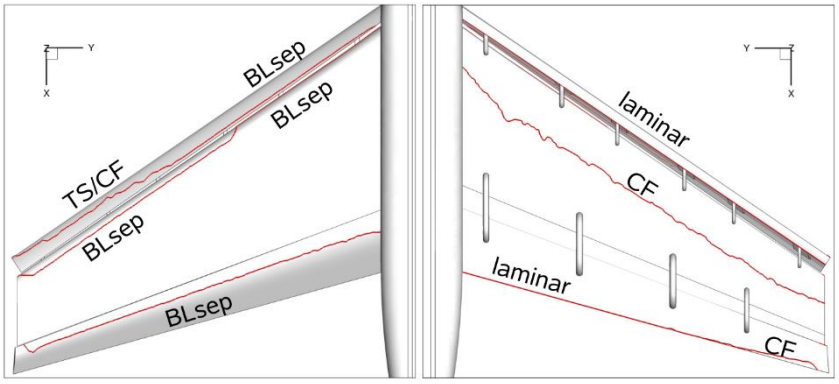

Figure 8 – Transition mechanism obtained by Crippa and Krimmelbein using stability analysis [34] (left: upper surface; right: lower surface)

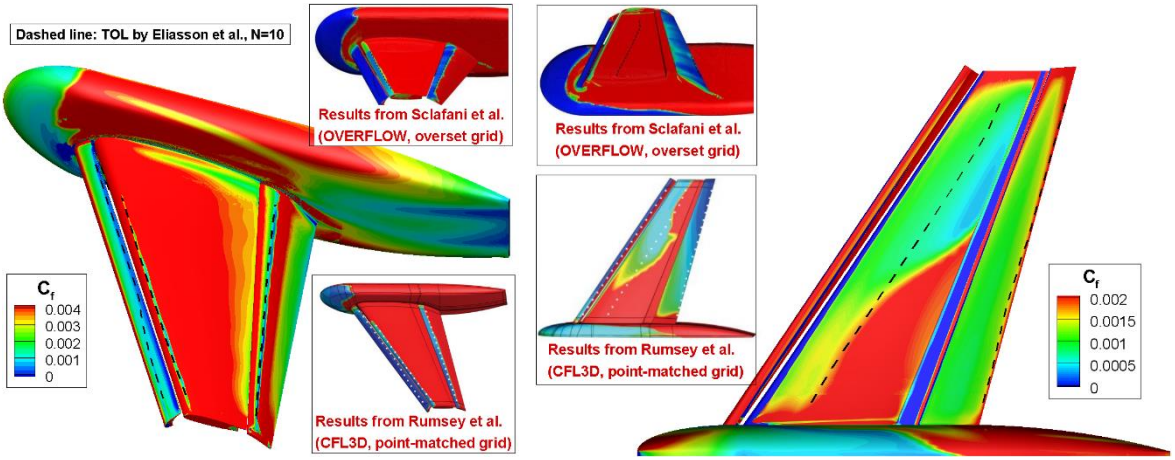

(a) Upper surface (b) Lower surface

Figure 9 – Predicted skin friction distribution and transition onset location of baseline $\gamma - \tilde{R}e_{\theta t}$ model comparing with reference results [35][36].

The overset grid generated for present work is shown in Fig. 10. The comparison of the computational pressure distributions of four spanwise sections and the streamwise sections near the leading and trailing edge of the flap are shown in Fig. 11. It can be found that the prediction accuracy of transition model is better than that of fully-turbulent simulation. Fig. 9 shows the predicted skin friction coefficient distribution of the upper and lower surfaces by baseline $\gamma - \tilde{R}e_{\theta t}$ transition model, and the reference result of Eliasson et al. (*N*=10) is also presented as comparison (black dotted line). The predicted TOLs of all the upper surfaces are basically consistent with the reference. The transition mechanism of the slat inner part, the main wing and the flap are all induced by separation (can be seen from the color of local C_f distribution), which is also consistent with the conclusion in Fig. 8. For lower surface, it can be seen that neither slat nor flap transition occurs, but the TOL of the main wing is quite different from the reference result, which is similar to that of Rumsey and Lee Rausch [35] who also used CFL3D solver.

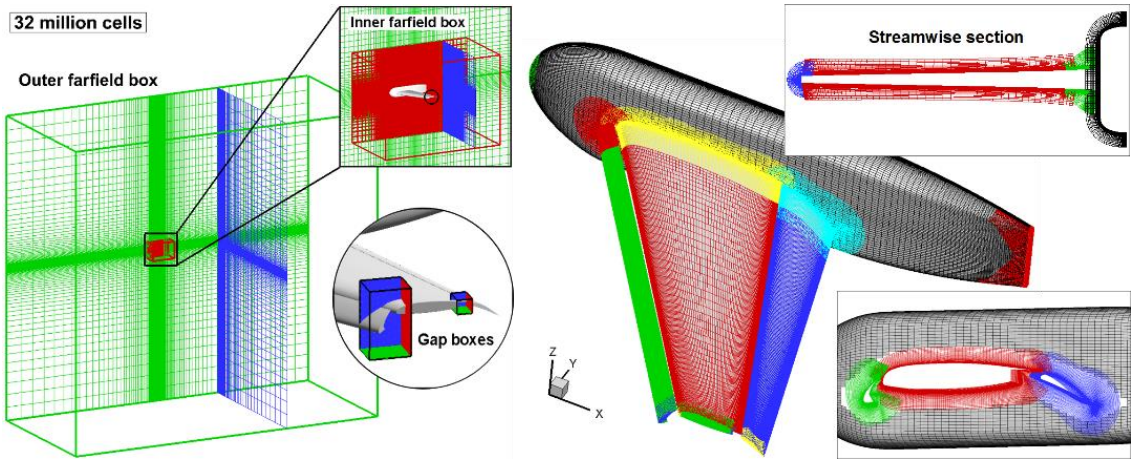

(a) Cartesian farfield and crack blocks at wingtip (b) Surface grid overlapping distribution

Figure 10 – Overset grid of NASA Trap Wing configuration.

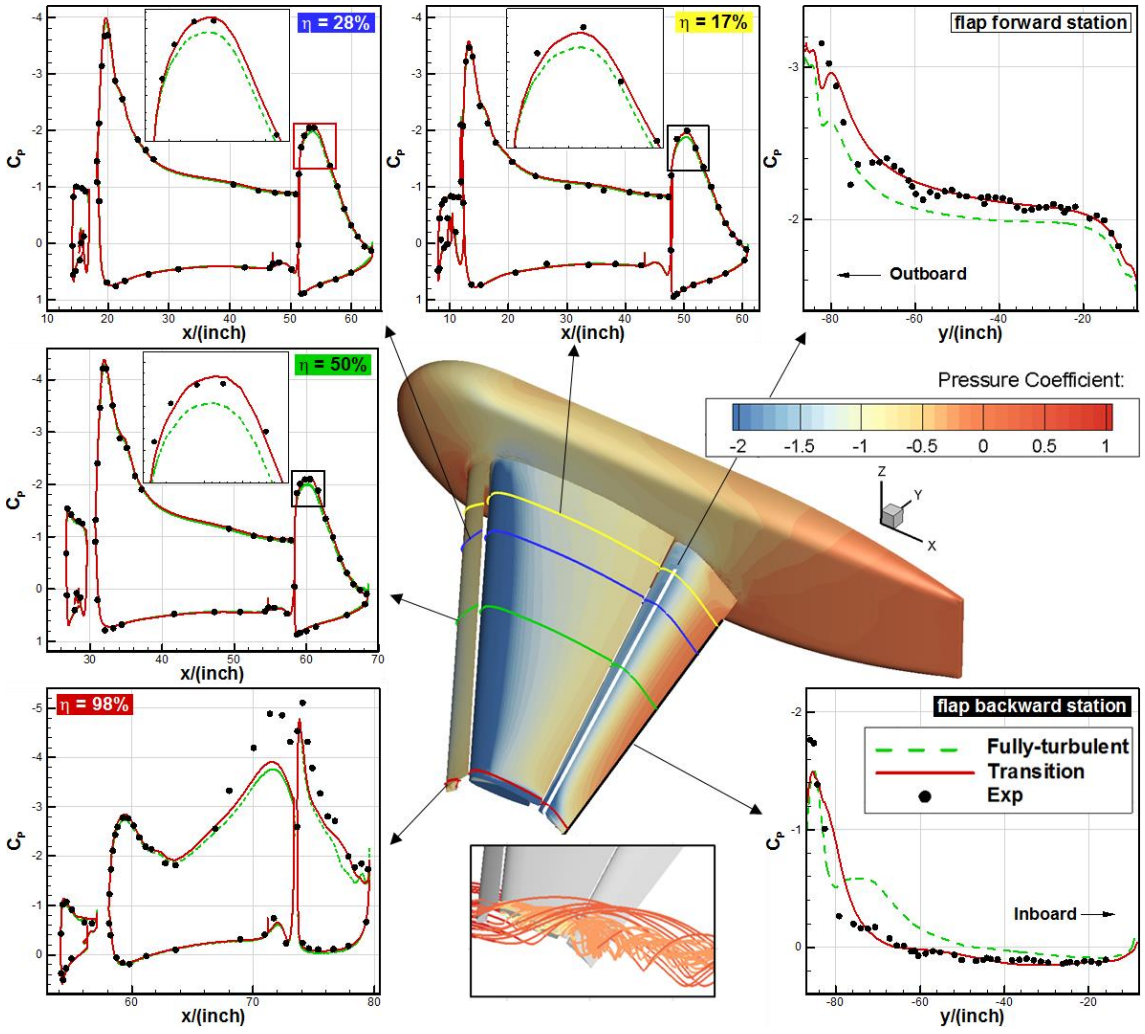

Figure 11 – Sectional pressure distribution comparison from different models with experiment.

Fig. 12 shows the skin friction coefficient distribution and TOL predicted by crossflow-extended transition model. It is obvious that the transition pattern on the lower surface of main wing is in good agreement with the reference results (closer to the result of *N*=10 [33]).

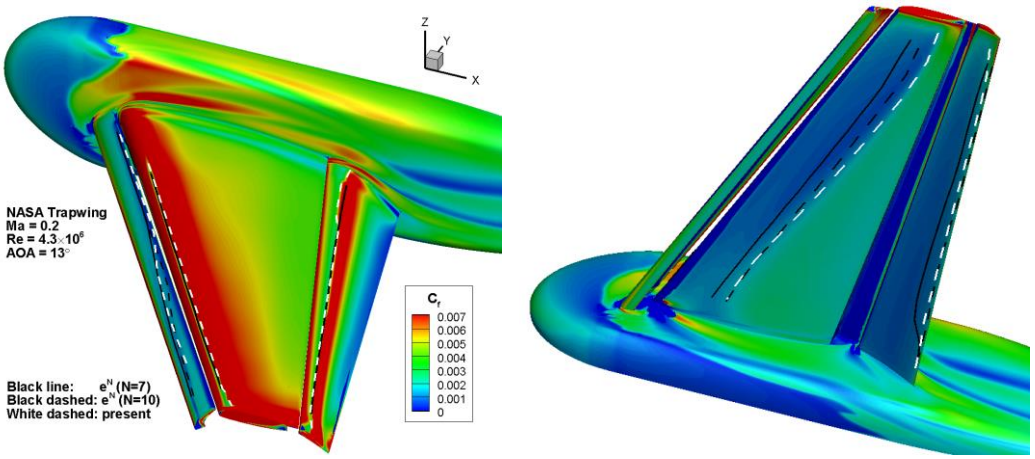

(a) Upper surface (b) Lower surface

Figure 12 – Predicted skin friction distribution and transition onset location of crossflow-extended $\gamma - \tilde{R}e_{\theta t}$ model

3.3 NASA CRM-NLF Configuration

Since 2017, NASA Langley Research Center (LaRC) has started natural laminar flow (NLF) design and experimental research on NASA General Research Model (CRM) [37]. The new model is called CRM-NLF. NASA LaRC adopted linear stability theory (LST) with other advanced design ideas and obtained *x*/*c*=50% laminar region (upper surface) on the whole span of a full-scale CRM-NLF model at *Re*=30×10^6 cruise condition. Compared with the original CRM full-scale model, the drag reduction is 6.8%, which greatly expands the application boundary of Reynolds number in the field of NLF design. It is one of the representative achievements in the society of civil aircraft design in recent years. The wind tunnel test was carried out at National Transonic Facility (NTF) [38], and the experiment model was 5.2% scaled (Fig. 13). Sectional pressure distributions were measured and the transition characteristics were visualized. In this paper, test case 2524 listed in Table 2 is selected. CRM-NLF is also one of the three-dimensional standard models of AIAA 1st CFD Transition Modeling and Prediction Workshop (TMPW-1).

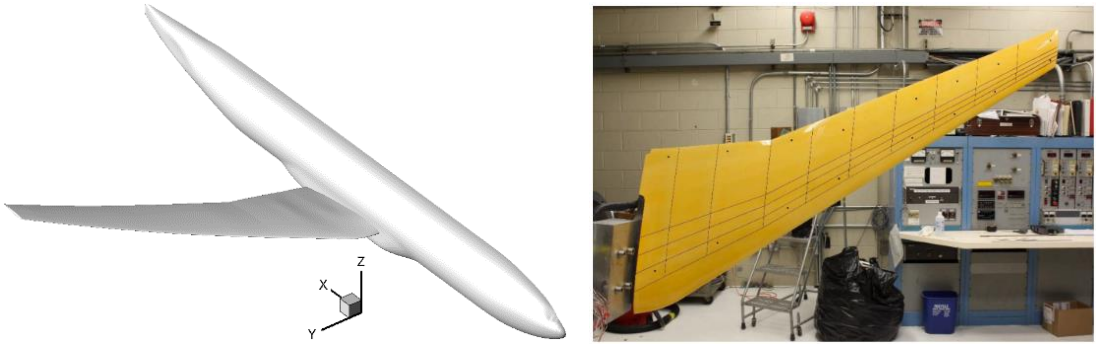

(a) CAD model (b) Wing of the wind-tunnel model

Figure 13 – NASA CRM-NLF configuration [38].

It can be seen from sectional pressure distribution comparisons in Fig. 14 that the results of the two transition models are basically consistent and in good agreement with experiment data. However, the predicted laminar region is much smaller than the experiment (Fig. 15).

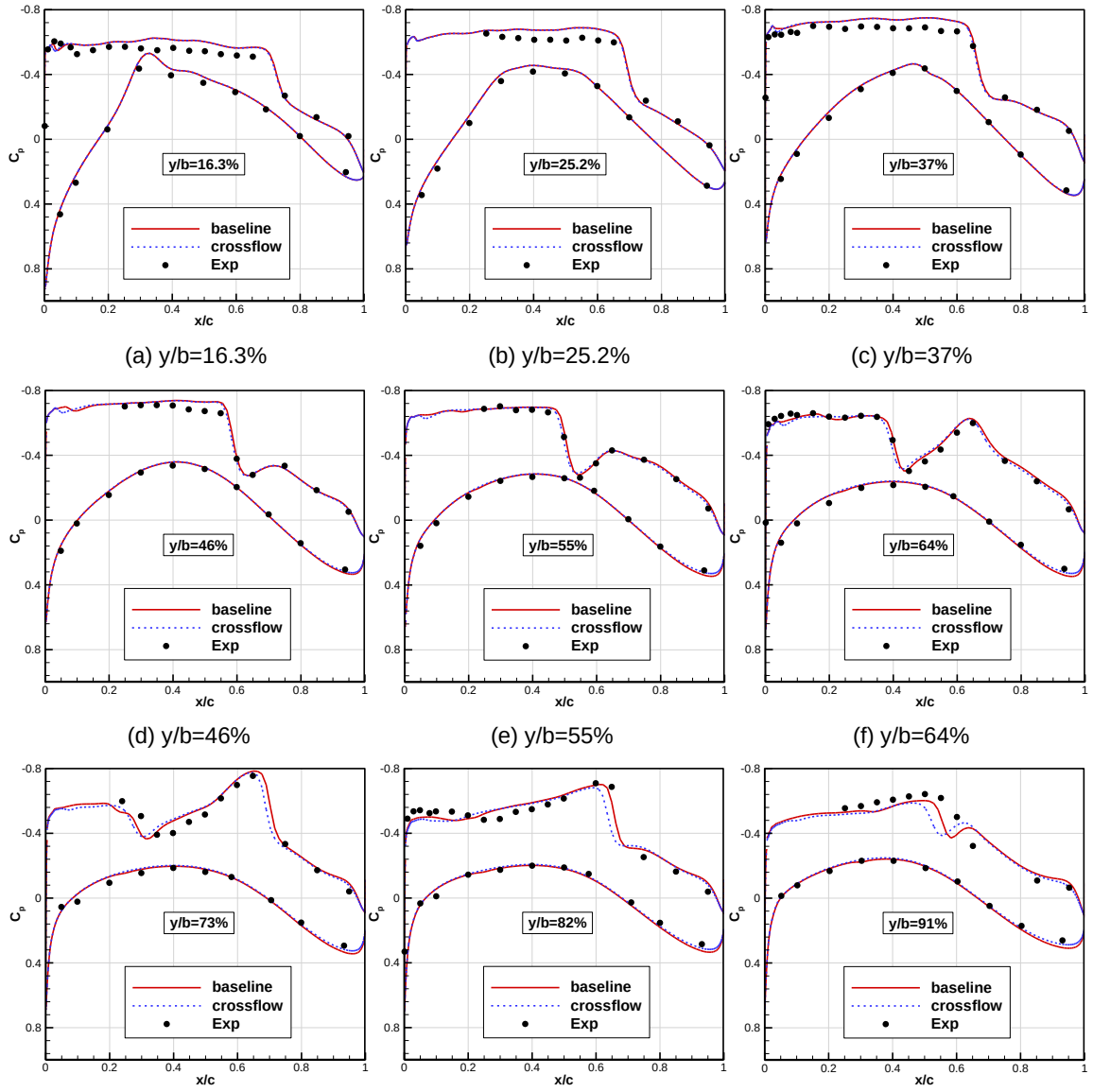

(a) y/b=16.3% (b) y/b=25.2% (c) y/b=37%

(d) y/b=46% (e) y/b=55% (f) y/b=64%

(g) y/b=73% (h) y/b=82% (i) y/b=91%

Figure 14 – Sectional pressure distribution comparison from different models with experiment.

The design target of CRM-NLF model is to eliminate the possible crossflow transition near the leading edge. From the flow visualization result in Fig. 15, the whole transition line on the upper wing should be controlled by T-S waves since there is no obvious "toothlike" transition line, which indicates transition induced by stationary crossflow vortices in the photo. Thus, the baseline $\gamma - \tilde{R}e_{\theta t}$ transition model gets a slightly larger laminar region and better predicted pressure distributions at the three sections near the wing tip. It can be inferred that the prediction difficulty of this case does not come from crossflow transition, but the high Reynolds number condition. This case basically prove that there should be an upper application boundary of Reynolds number for $\gamma - \tilde{R}e_{\theta t}$ transition model. For higher Reynolds number condition beyond the upper boundary, the authors think that the transition mechanisms described by empirical correlations, especially the T-S related part, are not applicable and the prediction results is not credible any more.

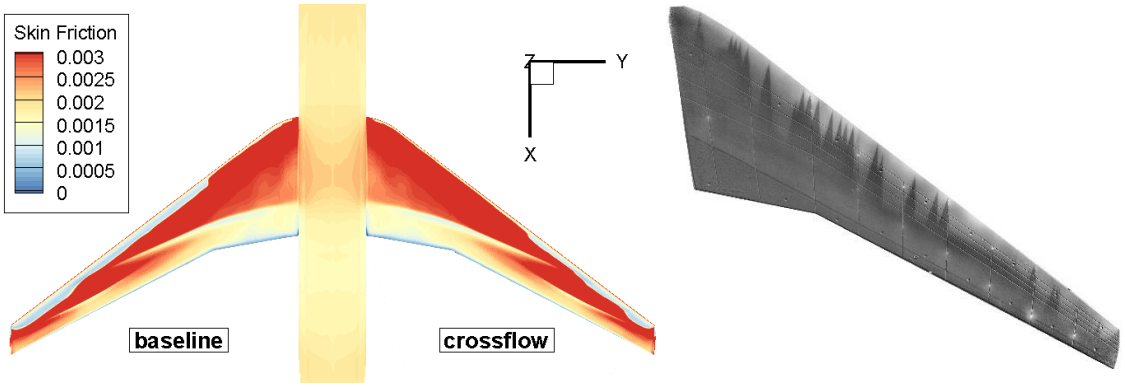

(a) Computational result (b) Experiment result by oil flow

Figure 15 – Predicted skin friction distribution and transition onset location comparison from different models with experiment.

4. Conclusions and Prospects

This paper established a comprehensive transition prediction method that applicable for civil transport aircraft configurations. The $\gamma - \tilde{R}e_{\theta t}$ local correlation-based transition model and a helicity-based crossflow transition criteria were introduced. Overset meshing strategy was adopted to deal with the grid generation challenge for complex configurations. Main conclusions and related prospects are as follows:

(1) The crossflow transition extension by the concept of helicity is suitable for transition prediction of arbitrary three-dimensional shapes. The stronger effect of crossflow instabilities at the inner part of wing and complex transition patterns of high-lift configuration can be accurately reflected, which validates the effectiveness of this method.

(2) Overset grid is a good alternative to conventional 1-1-blocking grid. It can not only reduce the grid generation difficulties, but also ensure reasonable grid distribution and good mesh orthogonality near the surface. But for very complex geometries, the overset meshing strategy may also suffer from topology difficulty and interpolation problem, which needs further improvement.

(3) The $\gamma - \tilde{R}e_{\theta t}$ transition model as well as its extension has an application upper boundary of Reynolds number. Experiment at high Reynolds number conditions needs to be conducted to obtain credible correlations. This is the basic premise for laminar flow design of civil transport aircraft using RANS transition model.

References

[1] Green J E. Laminar Flow Control – Back to the Future? AIAA paper 2008-3738, 2008.

[2] Braslow A L. A History of Suction-Type Laminar-Flow Control with Emphasis on Flight Research. Washington DC: NASA History Division of Office of Policy and Plans, Monographs in Aerospace History No.13, 1999.

[3] Menter F R, Esch T, Kubacki S. Transition model based on local variables. *5th International Symposium on Engineering Turbulence Modelling and Measurement*, Mallorca, Spain, 2002.

[4] Langtry R B, Menter F R. Correlation-Based Transition Modeling For Unstructured Parallelized Computational Fluid Dynamics Codes. *AIAA Journal*, Vol.47, No.12, pp 2894–2906, 2009.

[5] Fujino M. Design and Development of the HondaJet. *Journal of Aircraft*, Vol.42, No.3, pp 755-764, 2005.

[6] Benek J A, Steger J L, Dougherty F C, et al. Chimera: A Grid-Embedding Technique. AEDC-TR-85-64, 1986.

[7] Chandar D J, Boppana B L, Kumary V. A Comparative Study of Different Overset Grid Solvers Between OpenFOAM, STAR-CCM+ and ANSYS-Fluent. AIAA paper 2018-1564, 2018.

[8] Schlichting H, Gersten K. Boundary Layer Theory, 9th edition. Berlin Heidelberg: Springer-Verlag, 2017.

[9] Arnal D, Habiballah M, Coustols E. Laminar instability theory and transition criteria in two and three-

dimensional flows. *La Recherche Aerospatiale*, Vol.2, pp 45-63, 1984.

[10] Huang J T. Aircraft Aerodynamic Design and Aeroelasticity Analysis Based on CFD Numerical Simulation. Post-doctoral research report, Xi'an: Northwestern Polytechnical University, 2014 [Chinese].

[11] Krist S L, Biedron R T, Rumsey C L. CFL3D User's Manual-Ver. 5.0. 2nd edition. Hampton, Virginia: NASA Langley Research Center, NASA/TM-1998-208444, 1998. Also "the CFL3D Version 6 Home Page", NASA Langley Research Center, available at: https://cfl3d.larc.nasa.gov.

[12] Menter F R, Kuntz M, Langtry R. Ten Years of Industrial Experience with the SST Turbulence Model. Turbulence, Heat and Mass Transfer 4; Begell House, Inc., pp 625-632, 2003.

[13] Benek J A, Steger J L, Dougherty F C, and Buning P G. Chimera: A Grid-Embedding Technique. Arnold Air Force Station, Arnold Engineering Development Center, Rept. AEDC-TR-85-64, 1986.

[14] Baysal O, Fouladi K, and Lessard V R. A Multigrid and Upwind Viscous Flow Solver on 3-D Overlapped and Embedded Grids. AIAA paper 1989-464, 1989.

[15] Yu Y G, Zhou Z, Huang J T, Mou B, Huang Y, Wang Y T. Aerodynamic design of a standard model CHN-T1 for single-aisle passenger aircraft. *Acta Aerodynamica Sinica*, Vol. 36, No. 3, pp 505-513, 2018 [Chinese].

[16] Li Q, Liu D W, Xu X, et al. Experimental study of aerodynamic characterictics of CHN-T1 standard model in 2.4m transonic wind tunnel. *Acta Aerodynamica Sinica*, Vol. 37, No. 2, pp 337-344, 2019 [Chinese].

[17] Du Y M, Pang C, Shu B W, Gao Z H. Numerical simulation of the standard model CHN-T1 based on overset grid. *Acta Aerodynamica Sinica*, Vol. 37, No. 2, pp 280-290, 2019 [Chinese].

[18] Li W, Wang Y T, Hong J W, et al. Aerodynamic characteristics simulation of CHN-T1 model with TRIP3.0. *Acta Aerodynamica Sinica*, Vol. 37, No. 2, pp 272-279, 2019 [Chinese].

[19] Saric W S, Reed H L, White E B. Stability and transition of three-dimensional boundary layers. *Annual Review of Fluid Mechanics*, Vol.35, pp 413-440, 2003.

[20] Arnal D, Casalis G. Laminar-turbulent transition prediction in three-dimensional flows. *Progress in Aerospace Sciences*, Vol.36, pp 173-191, 2000.

[21] Dagenhart J R, Saric W S. Crossflow stability and transition experiments in swept-wing flow. Washington DC: NASA, NASA/TP-1999-209344, 1999.

[22] Crouch J D, Ng L L. Variable N-factor method for transition prediction in three-dimensional boundary layers. *AIAA Journal*, Vol.38, No.2, pp 211-216, 2000.

[23] Du Y M, Gao Z H, Wang C, Huang Q H. Boundary-layer transition of advanced fighter wings at high-speed cruise conditions. *Chinese Journal of Aeronautics*, Vol.32, No.4, pp 799-814, 2019.

[24] Grabe C, Nie S Y, Krumbein A. Transition Transport Modeling for the Prediction of Crossflow Transition. AIAA paper 2016-3572, 2016.

[25] Müller C, Herbst F. Modelling of crossflow-induced transition based on local variables. 6th European Conference on Computational Fluid Dynamics (ECFD VI), Barcelona, 2014.

[26] Langtry R B, Sengupta K, Yeh D T, Dorgan A J. Extending the γ-$Re_{\theta t}$ Local Correlation based Transition Model for Crossflow Effects. AIAA paper 2015-2474, 2015.

[27] Du Y M. Research on Corrections of RANS Eddy-Viscosity Turbulence Model and Prediction Method of Three-Dimensional Boundary-Layer Transition. Ph.D. dissertation, Xi'an: Northwestern Polytechnical University, 2021 [Chinese].

[28] Langlois M, Masson C, Paraschivoiu I. Fully three-dimensional transition prediction on swept wings in transonic flows. *Journal of Aircraft*, Vol.35, No.2, pp 254-259, 1998.

[29] Langlois M, Masson C, Kafyeke F, Paraschivoiu I. Automated method for transition prediction on wings in transonic flows. *Journal of Aircraft*, Vol.39, No.3, pp 460-468, 2002.

[30] Krimmelbein N, Krumbein A, Grabe C. Validation of Transition Modeling Techniques for a Simplified Fuselage Configuration. AIAA paper 2018-0030, 2018.

[31] Johnson P, Jones K, Madson M. Experimental Investigation of a Simplified 3D High Lift Configuration in Support of CFD Validation. AIAA paper 2000-4217, 2000.

[32] McGinley C B, Jenkins L N, Watson R D, Bertelrud A. 3-D High-Lift Flow-Physics Experiment-Transition Measurements. AIAA paper 2005-5148, 2005.

[33] Eliasson P, Hanifi A, Peng S-H. Influence of Transition on High-Lift Prediction for the NASA Trap Wing Model. AIAA paper 2011-3009, 2011.

[34] Crippa S, Krimmelbein N. Transitional Flow Computations of the NASA Trapezoidal Wing with the DLR

TAU Code. AIAA paper 2012-2845, 2012.

[35] Rumsey C L, Lee-Rausch E M. NASA Trapezoidal Wing Computations Including Transition and Advanced Turbulence Modeling. *Journal of Aircraft*, Vol.52, No.2, pp 496-509, 2015.

[36] Sclafani A J, Slotnick J P, Vassberg J C. Extended OVERFLOW Analysis of the NASA Trap wing Wind Tunnel Model. AIAA paper 2012-2919, 2012.

[37] Lynde M N, Campbell R L. Computational Design and Analysis of a Transonic Natural Laminar Flow Wing for a Wind Tunnel Model. AIAA paper 2017-3058, 2017.

[38] Rivers M B, Lynde M N, Campbell R L, etc. Experimental Investigation of the NASA Common Research Model with a Natural Laminar Flow Wing in the NASA Langley National Transonic Facility. AIAA paper 2019-2189, 2019.

Copyright Statement